Mechanisms of Oscillations and Formation of Nano-Scale Layered Structures in Induced Co-Deposition of Some Iron-Group Alloys (Ni−P, Ni−W, and Co−W), Studied by an In Situ Electrochemical Quartz Crystal Microbalance Technique

Sho-ichiro Sakai, Shuji Nakanishi, and Yoshihiro Nakato*

Division of Chemistry, Graduate School of Engineering Science, Osaka University, Toyonaka, Osaka 560-8531, Japan

Received: March 1, 2006; In Final Form: May 4, 2006

We have investigated mechanisms of oscillations and formation of nano-scale layered structures in induced co-deposition of some iron-group alloys (Ni−P, Ni−W, and Co−W) that have unique properties and are widely used in industries. Detailed in situ electrochemical quartz crystal microbalance (EQCM) experiments have revealed that the electrodeposition (induced co-deposition) of the alloys has negative differential resistances (NDRs), from which the oscillations and the layer-structure formation arise. The NDRs, however, cannot necessarily be seen in current−potential curves owing to overlap of hydrogen evolution current, indicating that the oscillations are of a hidden-NDR (H-NDR) type. The EQCM experiments have also shown that electrolyte components (such as $H_2PO_2^-$ and WO_4^{2-}) or related species are adsorbed at the electrode (deposit) surface and act as a promoter for the co-deposition reaction and that the NDRs arise from desorption of the adsorbed promoter. Interestingly, the adsorbed promoter is drawn into the deposition reaction itself, thus resulting in the alloy deposits. This mechanism was supported by in situ EQCM investigations of the oscillation as well as Auger electron spectroscopic (AES) analyses of deposits formed during the oscillation. The present work has for the first time clarified a general mechanism for the induced co-deposition reactions of some industrially important iron-group alloys (Ni−P, Ni−W, and Co−W).

1. Introduction

Alloys of iron-group metals (Fe, Co, and Ni) with other metallic or nonmetallic elements (P, Mo, and W), such as Fe−P, Co−W, Ni−P, and Ni−W, hereafter called iron-group alloys, are widely used in industries owing to their unique properties such as high corrosion resistance,[1−3] strong hardness,[1−3] brilliant luster for decoration,[1−3] electrocatalytic activity for hydrogen evolution,[4,5] and interesting magnetic properties such as magnetism/nonmagnetism transitions.[6] The studies made thus far[1−6] have also clarified that the incorporated elements (P, Mo, and W) in the alloys play the crucial role in their unique properties.

The iron-group alloys are mainly produced either by electroless deposition[1−3,6] or by electrodeposition.[4,5] It is known that the incorporated elements such as P, Mo, and W cannot be electrodeposited by themselves independently. However, interestingly, the elements can be co-deposited with iron-group metals, resulting in the iron-group alloys. This phenomenon is called "induced co-deposition".[7] The electrochemical deposition of the iron-group alloys is now widely used in industries, as mentioned above, but knowledge on the deposition mechanism is quite limited though such knowledge is very important for controlling the chemical composition, layered structures (explained later), and properties of the alloys. To date, several workers[7−12] have tried to explain the mechanism for the induced co-deposition, but, to our knowledge, all the reported models still remain only tentative or purely speculative. The purpose of the present work is thus to clarify the mechanism of the induced co-deposition with experimental evidence.

The induced co-deposition of the iron-group alloys has another interesting aspect in that it leads to layered structures, in which the iron-group metals and the incorporated elements change their contents periodically. The formation of the layered structures was commonly observed in all the reported induced co-deposition systems.[7,12,13] This result suggests that the induced co-deposition has a common general mechanism. It was also reported that an electrochemical oscillation was observed when the layered Ni−P alloy was codeposited.[14] The appearance of oscillations might also be characteristic of the induced co-deposition.

The formation of layered deposits, accompanied by oscillations, is known in other electrodeposition systems than the induced co-deposition. Schlitte et al. reported that the electrodeposition of Cu from an acidic Cu^{2+} solution containing an organic amine[15] showed an oscillation and gave a layered structure in the deposit. Recently, Switzer et al. reported that the oscillatory electrodeposition of Cu in an alkaline solution gave alternate Cu and Cu_2O layers with the unit-layer thickness of about 90 nm.[16,17] However, no mechanism has been revealed in these systems, too, until our recent work.[18−20] We have succeeded in revealing the mechanisms for the oscillatory electrodeposition of layered Cu metal[18] (a similar system to that reported by Schlitte et al.[15]) and layered Cu−Sn alloy.[19,20] The key in the success lay in that we were able to clarify the presence and the origin of negative differential resistances (NDRs), from which oscillations and layered-deposit formation appear.[21,22]

In the present work, we have adopted an electrochemical quartz crystal microbalance (EQCM) technique, together with normal electrochemical methods, to reveal the NDR in the induced co-deposition. The EQCM has proved to be quite

* To whom correspondence should be addressed. Tel: +81-6-6850-6235. Fax: +81-6-6850-6236. E-mail: nakato@chem.es.osaka-u.ac.jp.

10.1021/jp061282d CCC: $33.50
Published on Web 05/28/2006

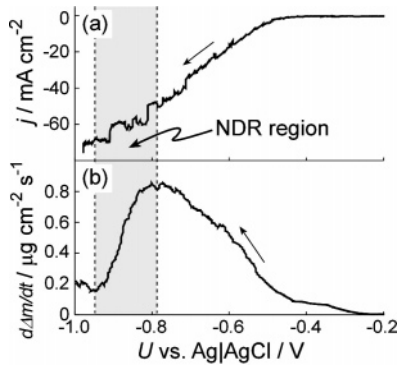

Figure 1. (a) j vs U obtained with the EQCM-Au electrode in an electrolyte of 0.65 M $NiSO_4$ + 0.25 M NaH_2PO_2 + 0.5 M H_3PO_4 + 0.3 M H_3BO_3 + 0.35 M NaCl (pH ≅ 1) under potential-controlled conditions, and (b) dΔm/dt vs U obtained simultaneously with the measurement of the j vs U in part a. The scan rate was 10 mV/ s.

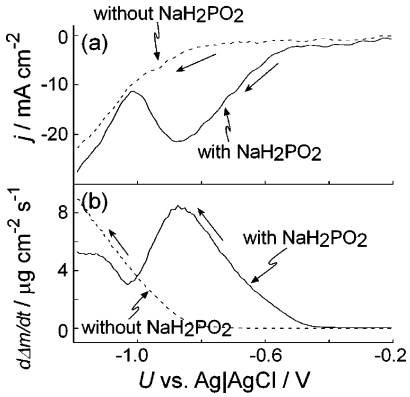

Figure 2. (a) j vs U in 0.65 M $NiSO_4$ + 0.3 M H_3BO_3 + 0.35 M NaCl in the absence (dashed-curve) and the presence (solid-curve) of 0.25 M NaH_2PO_2, and (b) the dΔm/dt vs U obtained simultaneously with the j *vs* U in part a. The scan rate was 10 mV/s.

effective to find the NDR in the induced co-deposition. The clarification of the NDR has enabled us to establish the essential mechanism for the induced co-deposition.

2. Experimental Section

In situ electrochemical quartz crystal microbalance (EQCM) experiments were done with a quartz crystal analyzer (USI SYSTEM, EQ200A). A commercially available 8 MHz AT-cut quartz crystal with thin Au layers on the front and rear faces, hereafter called an EQCM-Au electrode, was used as the working electrode for the EQCM experiments. The quartz crystal was installed in a Teflon holder so that only one Au face with the area of 0.20 cm^2 was exposed to the electrolyte. In some experiments, a polycrystalline Au (99.99% in purity) disk of 8 mm in diameter was used as the working electrode. A Pt plate (10 × 10 mm^2) and an Ag|AgCl|sat. KCl electrode were used as the counter and the reference electrodes, respectively. The electrolytes were prepared using special grade chemicals and pure water, the latter of which was obtained by purification of deionized water with a Milli-Q water purification system. The electrolyte temperature was kept at 70 °C.

Current density (j) vs potential (U) curves and j vs time (t) curves were recorded digitally at 1 kHz with a data-storing system (instruNET, GW instruments). No correction was made for ohmic drops in the electrolyte in the present work. Analyses of the chemical composition of electrodeposits were carried out with a scanning Auger electron spectroscopy (AES, JEOL, JAMP-7820F) combined with an Ar-ion etching technique. The accelerated voltage in the scanning AES was 10 kV.

3. Results

Figure 1a shows the j vs U in an electrolyte of 0.65 M $NiSO_4$ + 0.25 M NaH_2PO_2 + 0.5 M H_3PO_4 + 0.3 M H_3BO_3 + 0.35 M NaCl (pH ≅ 1), obtained with an EQCM-Au electrode (see the Experimental Section) in a negative potential scan under potential-controlled conditions. This electrolyte system was used previously by Vakhidov et al. for the electrodeposition of NiP alloy accompanied by an oscillation.[23] The current density (j) in Figure 1a starts to appear at about −0.45 V and monotonically increases (in the absolute value) with a negative potential shift. Concurrently with the measurement of the j vs U in Figure 1a, we also measured the frequency shift (Δf) in the EQCM, caused by a mass change (Δm) in the EQCM-Au electrode. Figure 1b shows the derivative of the Δm with respect to the time (t), dΔm/dt, calculated from the Δf. Because the Δm can be attributed to the Ni−P alloy electrodeposition in this electrolyte system, as argued later, the dΔm/dt is in proportion to the rate of the Ni−P alloy deposition. We can thus see from Figure 1b that the rate of the Ni−P alloy deposition increases monotonically with a negative potential shift in a U range from −0.45 to −0.80 V, whereas it suddenly starts to decrease at around −0.80 V and continues to decrease until it reaches about −0.95 V, in contrast to the current density in Figure 1a. This implies that the Ni−P alloy deposition current has a negative differential resistance (NDR) in the U range of $-0.95\ \text{V} < U < -0.80\ \text{V}$, which we hereafter call the U_{NDR} region. The j vs U in Figure 1a does not show any NDR, which is most probably because the NDR is hidden by an overlap of a hydrogen evolution current (argued later), which increases (with a negative potential shift in this U range) more steeply than the decrease in the Ni−P alloy deposition current.

The solid curve in Figure 2a shows the j vs U in another electrolyte of 0.65 M $NiSO_4$ + 0.25 M NaH_2PO_2 + 0.3 M H_3BO_3 + 0.35 M NaCl, in which 0.5 M H_3PO_4 is missing compared with the electrolyte of Figure 1. This electrolyte has a higher pH (pH ≅ 4) than that used in Figure 1 (pH ≅ 1), which implies that the hydrogen evolution current in Figure 2a should shift to more negative potentials than in Figure 1. The dashed curve in Figure 2a is for the absence of 0.25 M NaH_2PO_2 (the P-source in the Ni−P alloy). In the presence of NaH_2PO_2 (solid curve), the current started to flow at about −0.5 V, in the same way as in Figure 1a, but the NDR was observed in the j vs U, contrary to the case of Figure 1a. This is mainly due to removal of the overlap of the hydrogen evolution current by its negative shift, mentioned above. In the absence of NaH_2PO_2 (dashed curve), the current started to flow at a more negative potential than in the presence of NaH_2PO_2 and shows no NDR. It is to be noted that the j values in the presence and the absence of NaH_2PO_2 became nearly the same in a U range more negative than −1.0 V (or U_{NDR}). This implies that the added NaH_2PO_2 has almost no effect on the deposition reaction in this U range.

Figure 3a shows a time course of a potential oscillation, which appeared spontaneously when the j was kept at a constant value in a range of $-55 < j < -75\ \text{mA cm}^{-2}$, i.e., in a range of j when U was in the U_{NDR} region of Figure 1a. The electrolyte was the same as that in Figure 1, but an Au-plate was used as the working electrode in this case. It may be noted that the highest and lowest values of the oscillating potential in Figure 3a nearly coincide with the highest and lowest potentials of the U_{NDR} region, respectively. The potential oscillation observed with the EQCM-Au electrode is shown in Figure 3b. Nearly the same potential oscillation as Figure 3a was observed, though

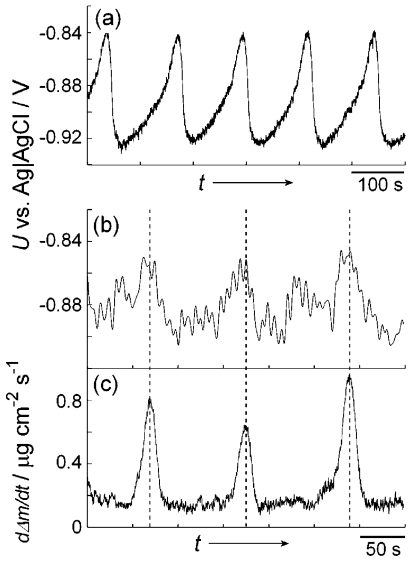

Figure 3. (a) U vs t at a constant j of -75 m Acm^{-2}, obtained in the same electrolyte as Figure 1 with an Au plate as the working electrode. (b) The same as part a, except that the EQCM-Au electrode is used. (c) dΔm/dt *vs* t obtained simultaneously with the measurement of the potential oscillation in part b.

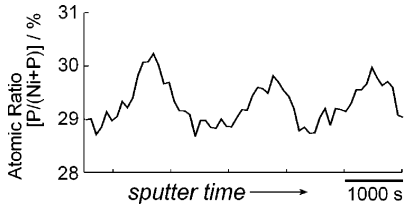

Figure 4. Auger depth profile for a deposit produced under the potential oscillation.

the oscillation in Figure 3b was strongly affected by hydrogen gas evolution at the electrode surface because the EQCM-Au electrode was installed in a Teflon holder in which detachment of hydrogen-gas bubbles was difficult. Figure 3c shows the dΔm/dt vs t, measured simultaneously with the potential oscillation of Figure 3b. Interestingly, the dΔm/dt, i.e., the Ni−P alloy deposition rate, oscillates synchronously with the potential oscillation. We can also note that the Ni−P deposition occurs at a much higher rate at the highest potential in the oscillation than at the lowest potential.

Figure 4 shows an Auger depth profile for a deposit film formed during the potential oscillation, in which 0.5 M citric acid was added as a surface flattening agent. The addition of citric acid caused no changes in the j vs U and the waveform of the potential oscillation. The atomic ratio, P/(Ni + P), was calculated from the corresponding AES peak intensities with corrections for the relative ionization efficiencies. The result of Figure 4 clearly shows that the Ni−P alloy with a layered structure is formed in the deposit. Furthermore, the number of the layers in the deposit agreed with the number of the cycles of the potential oscillation during which the deposit was formed, indicating that one oscillation cycle produced one layer of the deposit. The thickness of one layer was estimated to be a few hundred nanometers, by dividing the thickness of the deposit, measured with an optical microscope, by the number of the oscillation cycles.

To clarify the U dependence of the electrodeposition process, we investigated the depth profile for a deposit film formed (in the electrolyte of Figure 2) when U was first fixed at -1.2 V ($< U_{NDR}$ of Figure 2) for 30 s and then stepped to -0.85 V ($> U_{NDR}$) and kept at this potential for 30 s. Figure 5 shows the depth profile for the deposit thus prepared. We can see that the P content is high for the deposit formed at the positive potential and low at the negative potential. We did experiments similar to that above using the electrolyte of Figure 1 and confirmed that the P content in the Ni−P alloy decreased as the U was shifted toward the negative.

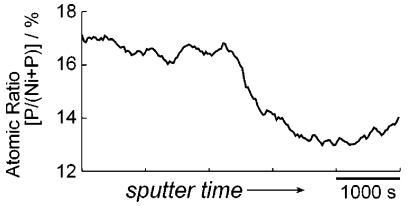

Figure 5. Auger depth profile for a deposit produced when U was first kept constant at -1.2 V for 30 s and then stepped to -0.85 V and kept at this potential for 30 s.

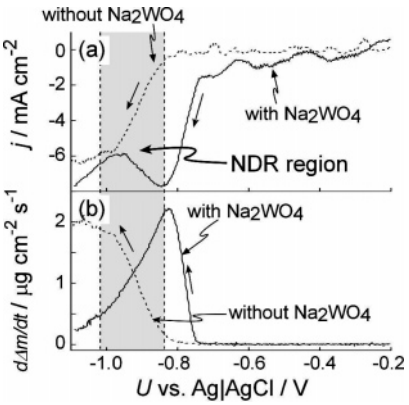

Figure 6. (a) j vs U in 0.1 M $CoSO_4$ + 0.25 M Na_2SO_4 + 0.1 M sodium citrate without (dashed-curve) and with (solid-curve) 50 mM Na_2WO_4, observed under the potential-controlled conditions, and (b) dΔm/dt vs U, obtained simultaneously with the measurement of the j vs U in part a. The scan rate was 10 mV/s.

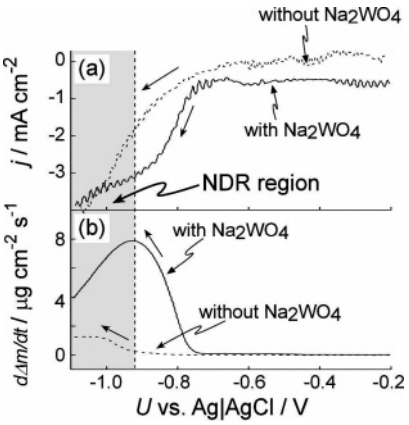

Figure 7. (a) j vs U in 0.1 M $NiSO_4$ + 0.25 M Na_2SO_4 + 0.1 M sodium citrate without (dashed-curve) and with (solid-curve) 50 mM Na_2WO_4, observed under the potential-controlled conditions, and (b) dΔm/dt vs U, obtained simultaneously with the measurement of the j vs U in part a. The scan rate was 10 mV/s.

In order also to investigate a generality of the mechanism for the formation of the iron-group alloys, we performed experiments in other induced co-deposition systems. Figures 6 and 7 show the results for the electrodeposition of Co−W and Ni−W alloys, respectively. Essentially the same behavior as for the Ni−P deposition was observed in these co-deposition systems. Namely, the deposition current in the presence of Na_2WO_4 (the W-source of the Co−W and Ni−W alloys) started to

flow at a more positive potential than in the absence of Na_2WO_4. Besides, the $d\Delta m/dt$ vs U in the presence of Na_2WO_4, where the $d\Delta m/dt$ is in proportion to the rate of the alloy deposition, showed the clear NDR, though the $d\Delta m/dt$ vs U in the absence of Na_2WO_4 showed no NDR. These results indicate that the electrodeposition of the Co−W and Ni−W alloys occurs by essentially the same mechanism as that of the Ni−P alloy, suggesting the presence of a general mechanism for the induced co-deposition of these alloys.

4. Discussion

In situ EQCM experiments have revealed that the induced co-deposition reactions for the Ni−P, Co−W, and Ni−W alloys all have the NDRs (Figures 1, 2, 6, and 7). However, the NDRs are not necessarily observed in the j vs U curves because they are sometimes hidden by the overlap of the hydrogen evolution current. Recent theoretical work[21,22] has indicated that the presence of the NDRs of both nonhidden and hidden types cause electrochemical oscillations under appropriate conditions. The oscillations in the former case are called NDR oscillators, whereas those in the latter case are called H-NDR (or hidden NDR) oscillators. The recent theoretical work[21,22] has also shown that only the current oscillations appear for the NDR oscillators, whereas both the current and the potential oscillations appear for the H-NDR oscillators. Thus, the oscillation appearing in the Ni−P alloy deposition can be classified into the H-NDR oscillator and its mechanism can be explained in terms of the H-NDR oscillator.

For clarifying the mechanisms for the oscillations and the formation of layered structures, it is of key importance to clarify not only the existence of the NDR but also the chemical origin of it. To begin with, we should note that the Ni−P alloy deposition current in the presence of NaH_2PO_2 starts to flow at a more positive potential than in the absence of NaH_2PO_2, as is clearly seen from Figure 2. This fact indicates that NaH_2PO_2 or a species related to it acts as a promoter for the Ni−P deposition reaction. In addition, the fact that the Ni−P alloy is formed (or NaH_2PO_2 is the P-source for the Ni−P alloy) indicates that the species acting as the promoter is drawn into the deposition reaction itself. This means that the promoter (NaH_2PO_2 or a related species) is present in the adsorbed form at the electrode (or deposit) surface.

The above considerations strongly suggest that the NDR, i.e., the decrease in the Ni−P alloy deposition current in the U_{NDR} region (Figure 1b or 2b), arises from desorption (detachment) of the adsorbed promoter in this potential region. The desorption of the adsorbed promoter may be caused by an increase in negative charges at the electrode surface by the negative potential shift.

Many examples are known[24−32] for the appearance of the NDRs via the desorption of an adsorbed promoter or catalyst for electrochemical reactions, though it has never been reported that the adsorbed promoter is drawn into the deposition reaction itself, as in the Ni−P alloy deposition. The incorporation of the adsorbed promoter into the deposition reaction implies that the adsorbed promoter has an ability to form a complex with Ni^{2+} ions in the electrolyte. A reduced form of adsorbed $H_2PO_2^-$, such as adsorbed $H_2P{-}O^-$ or H_2P^-, which has lone-pair electrons, may thus be a possible candidate for the adsorbed promoter. The desorption of the adsorbed promoter produces vacant sites at the electrode surface, at which normal electrodeposition of Ni metal can occur, though its deposition rate is much slower than that for the Ni−P deposition, as is seen from comparison of the solid and dashed curves in Figure 2b. This argument is supported by the aforementioned fact that the j values in the presence and the absence of NaH_2PO_2 become nearly the same as each other in a region of $U < U_{NDR}$, in which the adsorbed promoter is entirely desorbed.

The above mechanism is also in harmony with the fact that the P content in the deposit is decreased as the deposition potential gets more negative (Figure 5). The Ni-metal deposition at the vacant sites produced by the desorption of the adsorbed promoter will be more efficient with the negative potential shift, resulting in a decrease in the P content in the deposit.

Before starting discussion on the mechanism of the potential oscillation, let us consider some aspects to be investigated in the present deposition system. We mentioned earlier that the NDR in the Ni−P alloy deposition current (Figure 1b) was hidden in the j vs U of Figure 1a by the overlap of the hydrogen evolution current. The occurrence of the hydrogen evolution was clearly seen by formation of gas bubbles at the electrode surface. The occurrence of the hydrogen evolution was also seen by observation of fluctuating noisy currents in the j vs U curve (see Figure 1a), caused by gas-bubble formation at the electrode surface. The amplitude of the noisy current is increased as the U becomes more negative, suggesting that the hydrogen evolution gets more rigorous at more negative potentials.

In the electrolyte of Figure 2, on the other hand, almost no hydrogen evolution was observed, at least in $U \geq U_{NDR}$. Such a large difference in the hydrogen evolution efficiency between Figures 1 and 2 may not be explained by a small difference in the solution pH ($\Delta pH \cong 3$). We have to note here that the catalytic activity of the Ni−P alloy, denoted as NiP_x, for the hydrogen evolution is very sensitive to the x value and varies by several decades with x. For example, it is reported[4] that the hydrogen evolution on $NiP_{0.17}$ is over 100 times as efficient as that on $NiP_{0.23}$ in 1 M KOH. It is also reported[8] that the x value of the alloy strongly depends on the pH of the electrolyte from which the alloy is deposited. We also confirmed by the AES that the x value was around 0.30 in the electrolyte of $pH \cong 1$ (Figure 1) and 0.15 in the electrolyte of $pH \cong 4$ (Figure 2). Thus, we can conclude that a large difference in the hydrogen evolution efficiency between Figures 1 and 2 can partly be attributed to a difference in the atomic $P/(P + Ni)$ ratio of the deposited alloys.

Another aspect is that the rate of the Ni−P deposition, i.e., the $d\Delta m/dt$ value, in Figure 1b is very low, about one-tenth of that of Figure 2b. As mentioned above, the efficient hydrogen evolution occurs in the case of Figure 1b, which will lead to a large local increase in the solution pH near the electrode (deposit) surface. The local large increase in the pH will cause formation of metal oxide or hydroxide ($Ni_s{-}OH$) at the electrode (deposit) surface, leading to retardation of the Ni−P alloy deposition.[33−35] A number of examples are known[36−38] for the formation of metal oxide or hydroxide in metal-deposition systems, caused by an increase in the solution pH through the hydrogen evolution.

Now, let us consider the mechanism for the potential oscillation and formation of a layered structure in the Ni−P alloy deposition, observed under the galvanostatic condition with a constant applied j (Figure 3). Figure 8 schematically illustrates expected oscillatory changes in the coverage (θ) of the adsorbed promoter, the surface concentration (C_s) of Ni^{2+} ions, and the applied electrode potential (U). Let us start to consider stage-1 of Figure 8. At this stage, the potential (U) is the most positive of the potential oscillation and therefore the coverage (θ) of the adsorbed promoter is high (Figure 5), which leads to the high Ni−P alloy deposition rate. The occurrence of the high-

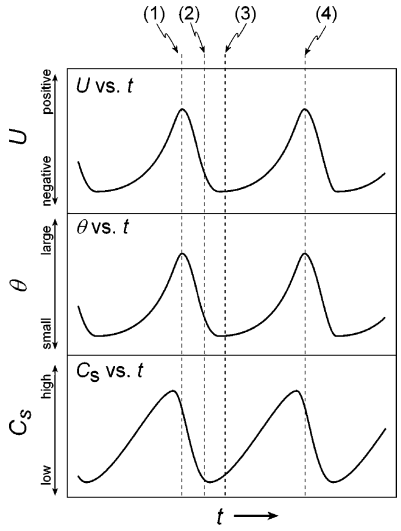

Figure 8. Schematic illustrations of expected oscillatory changes in U, θ, and C_s with t.

rate Ni−P deposition, on the other hand, leads to a decrease in the surface Ni^{2+} concentration (C_s) and thus causes a gradual negative U shift to keep the constant j. When U has shifted to the negative and reached the U_{NDR} region, the desorption of the adsorbed promoter starts. In this region, the negative U shift leads to a decrease in the coverage (θ) of the adsorbed promoter and to a decrease in the Ni−P alloy deposition current, which, in turn, leads to a further negative U shift to keep the constant j (stage-2). Here is an autocatalytic process. Thus, the potential rapidly goes to the negative end of the potential oscillation (stage-3).

At stage-3, at which the U is at the negative end of the potential oscillation, the adsorbed promoter is nearly absent at the electrode surface, and only the slow Ni−P and Ni deposition occurs, with the constant j being maintained by the hydrogen evolution. Thus, the C_s gradually increases by diffusion of Ni^{2+} ions from the electrolyte bulk. The increase in the C_s induces a gradual increase in the Ni−P alloy (and Ni metal) deposition current, which leads to a gradual positive shift in U to keep the constant j. When U has shifted to the positive and reached the U_{NDR} region, the adsorption of the promoter starts to occur, leading to an increase in the θ. In the U_{NDR} region, the positive shift in U leads to an increase in the θ and thus an increase in the Ni−P alloy deposition current, which, in turn, leads to a further positive U shift to keep the constant j. Here is also an autocatalytic process. Thus, the system rapidly goes back to the positive end of the potential oscillation (stage-4).

The experimentally observed in situ EQCM response is in good accordance with the above mechanism. In the positive-end of the potential oscillation, the Ni−P alloy deposition occurs efficiently because of the high θ. This implies that the $d\Delta m/dt$ is large at this stage, in agreement with the experiment (Figure 3c). On the other hand, in the negative-end of the potential oscillation, the θ is low and thus the Ni−P deposition is slow, in agreement with the low $d\Delta m/dt$ value at this stage (Figure 3c). The low Ni−P alloy deposition current is compensated by the hydrogen evolution current (which causes no mass change) to keep the constant j. The periodic modulation in the P content in the deposit formed under the potential oscillation (Figure 4) can also be explained by the decrease in the P content at the negative potentials, caused by the additional deposition of Ni metal at the negative potentials (Figure 5).

Although a large number of studies have been made on the *induced co-deposition*,[7−12] especially on the Ni−P alloy deposition,[8−11] any mechanisms thus far reported[8−11] were not able to explain the appearance of oscillations and formation of layered deposits on the reasonable background. The present work has, for the first time, revealed a reasonable mechanism with experimental evidence, which is in harmony with recent general theory on the electrochemical oscillations.[21,22] The results of Figures 6 and 7, in which the behavior of the $d\Delta m/dt$ is essentially the same as that for the Ni−P deposition, indicate that the above mechanism can be applied to the induced co-deposition of Ni−W and Co−W as well. The positive onset of the deposition current as well as the appearance of the NDR in the $d\Delta m/dt$ vs U in the presence of WO_4^{2-} (Figures 6 and 7) clearly indicate that adsorbed WO_4^{2-} or a related species acts as the promoter for the alloy deposition in these cases. Furthermore, the layer formation is commonly observed in various *induced co-deposition* systems.[7,12−14] These arguments strongly suggest that the present mechanism can be regarded as a general mechanism for the *induced co-deposition* of some iron-group alloys (Ni−P, Ni−W, and Co−W).

In conclusion, the present study has revealed a general mechanism for the *induced co-deposition* of some iron-group alloys (Ni−P, Ni−W, and Co−W). The co-deposition current has the NDR, as clearly shown by the measurements of the mass change, although the NDR is not necessarily observed in the j vs U curves owing to the overlap of other currents such as hydrogen evolution. The NDR for the co-deposition reaction appears from a mechanism that the adsorbed species acting as the promoter for the co-deposition is desorbed from the surface with the negative potential shift. The adsorbed species acting as the promoter is drawn into the deposition reaction itself, thus resulting in the formation of the alloys. The present mechanism will be useful for controlling the chemical composition, the size of the layered structures, and various properties of the alloys for high performances in industrial applications.

Acknowledgment. The present work is supported by the Grant-in-Aid for Scientific Research (KAKENHI) in Priority Area "Molecular Nano Dynamics" from Ministry of Education, Culture, Sports, Science and Technology. The authors also thank the Core Research for Evolutional Science and Technology (CREST) program of the Japan Science and Technology Agency (JST) for financial supports.

References and Notes

(1) Tulsi, S. S. *Trans. Inst. Met. Finish.* **1986**, *64*, 73.
(2) Parker, K. *Plat. Surf. Finish.* **1992**, *79*, 29.
(3) Williams, J. E.: Davison, C. *J. Electrochem. Soc.* **1990**, *137*, 3260.
(4) Paseka, I.; Velicka, J. *Electrochim. Acta* **1997**, *42*, 237.
(5) Burchardt, T. *Int. J. Hydrogen Energy* **2001**, *26*, 1193.
(6) Flis, J.; Duguatte, D. J. *J. Electrochem. Soc.* **1984**, *40*, 425.
(7) Brenner, A. *Electrodeposition of Alloys*; Academic Press: New York, 1963; Vol. 1−2.
(8) Morikawa, T.; Nakade, T. *Electrochim. Acta* **1997,** *42*, 115.
(9) Zeller, R. L.; Landau, U. *J. Electrochem. Soc.* **1992**, *139*, 3464.
(10) Harris, T. M.; Dong, Q. D. *J. Electrochem. Soc.* **1993**, *140*, 81.
(11) Ratzker, M.; Lashmore, D. S.; Pratt, K. W. *Plat. Surf. Finish.* **1986**, *73*, 74.
(12) Podlaha, E. J.; Landolt, D. *J. Electrochem. Soc.* **1996**, *143*, 885.
(13) Ogburn, F.; Johnson, C. E. *Plating* **1973**, *60*, 1043.
(14) Lee, W. G. *Plating* **1960**, *47*, 288.
(15) Schlitte, F.; Eichkorn, G.; Fischer, H. *Electrochim. Acta* **1968**, *13*, 2063.
(16) Switzer, J. A.; Hung, C. J.; Huang, L. Y.; Switzer, E. R.; Kammler, D. R.; Golden, T. D.; Bohannan, E. W. *J. Am. Chem. Soc.* **1998**, *120*, 3530.
(17) Bohannan, E. W.; Huang, L. Y.; Miller, F. S.; Shumsky, M. G.; Switzer, J. A. *Langmuir* **1999**, *15*, 813.
(18) Nakanishi, S.; Sakai, S.-I.; Nishimura, K.; Nakato, Y. *J. Phys. Chem. B* **2005**, *109*, 18846.
(19) Sakai, S.-I.; Nakanishi, S.; Fukami, K.; Nakato, Y. *Chem. Lett.* **2002**, *31*, 640.

(20) Nakanishi, S.; Sakai, S.-I.; Nagai, T.; Nakato, Y. *J. Phys. Chem. B* **2005**, *109*, 1750.
(21) Krischer, K. Principles of Temporal and Spatial Pattern Formation in Electrochemical Systems. In *Modern Aspects of Electrochemistry*; White, R. W., Bockris, O. M., Conway, R. E., Eds.; Plenum: New York, 1995; Vol. 32, p 1.
(22) Strasser, P.; Eiswirth, M.; Koper, M. T. M. *J. Electroanal. Chem.* **1999**, *478*, 50.
(23) Vakhidov, R. S.; Popov, V. I. *Elektrokhimiya* **1970**, *6*, 1720.
(24) de Levie, R. *J. Electrochem. Soc.* **1970**, *118*, 185C.
(25) Pospisil, L.; de Levie, R. *J. Electroanal. Chem.* **1970**, *25*, 245.
(26) Jurczakowski, R.; Orlik, M. *J. Phys. Chem. B* **2002**, *106*, 1058.
(27) Jurczakowski, R.; Orlik, M. *J. Phys. Chem. B* **2003**, *107*, 10148.
(28) Nakanishi, S.; Mukouyama, Y.; Karasumi, K.; Imanishi, A.; Furuya, N.; Nakato, Y. *J. Phys. Chem. B* **2000**, *104*, 4181.
(29) Mukouyama, Y.; Nakanishi, S.; Chiba, T.; Murakoshi, K.; Nakato, Y. *J. Phys. Chem. B* **2001**, *105*, 7246.
(30) Nakanishi, S.; Sakai, S.-I.; Hatou, M.; Mukouyama, Y.; Nakato, Y. *J. Phys. Chem. B* **2005**, *106*, 2287.
(31) Nakanishi, S.; Sakai, S.-I.; Fukami, K.; Mukouyama, Y.; Nakato, Y. *J. Electrochem. Soc.* **2003**, *150*, E47.
(32) Nakanishi, S.; Mukouyama, Y.; Nakato, Y. *J. Phys. Chem. B* **2001**, *105*, 5751.
(33) Dahms, D.; Croll, I. M. *J. Electrochem. Soc.* **1965**, *112*, 771.
(34) Lieder, M.; Biallozor, S. *Surf. Coat. Technol.* **1998**, *26*, 23.
(35) Sasaki, K. Y.; Talbot, J. B. *J. Electrochem. Soc.* **2000**, *147*, 189.
(36) Nataragan, C.; Nogami, G. *J. Electrochem. Soc.* **1996**, *143*, 1547.
(37) Gal-Or, L.; Silberman, I.; Chaim R. *J. Electrochem. Soc.* **1991**, *138*, 1939.
(38) Switzer, J. A. *Am. Ceram. Bull.* **1987**, *66*, 1521.